Field and theoretical investigation of sediment mass fluxes on an accretional coastal mudflat

Benwei Shi [a], Ya Ping Wang [a *], Xiaoqin Du [a], James R. Cooper [b], Peng Li [c], Ming Liang Li [d], Yang Yang[a]

[a]*Ministry of Education Key Laboratory for Coast and Island Development, Nanjing University, Nanjing 210093, China*

[b]*Department of Geography and Planning, School of Environmental Sciences, University of Liverpool, Liverpool, UK.*

[c] *Forecast Center for East China Sea, SOA, Shanghai 200081, China*

[d]*Geological Survey of Jiangsu Province, Nanjing, Jiangsu, 210018, China*

Corresponding author information,

Telephone: 086-025-83686010;

Fax: 086-025-83595387;

Email address: ypwang@nju.edu.cn (Y. P. Wang).

Abstract Variations in suspended sediment concentrations (SSCs) in tidal mudflats are an important influence on the ecological environment, morphological evolution, and pollutant transport. To better understand how the behavior of suspended sediment influences small-scale variations in SSC in the water column, we took simultaneous measurements of water depth, wave height, current velocity, SSC profiles, and intratidal bed-level changes during a series of continuous tidal cycles on a highly turbid macrotidal mudflat, part of a larger accretional coastal mudflat on the Jiangsu Coast, China. We estimated the relative contributions of erosion, deposition, and advection processes to variations in SSC from the field data. We used an empirical orthogonal function (EOF) analysis to examine the influence of hydrodynamic factors (water depth, wind, wave height, and current velocity) and environmental factors (salinity and temperature) on SSC variability, to determine why the contributions of the three processes (erosion, deposition, and advection) to the variability in SSC differed. Our results showed that on average advection flux was about an order of magnitude higher than erosion-deposition flux of corresponding tide, and that advection, driven by the tidal current velocity, wind, and associated alongshore transport, accounted for most of the variability in SSC at the study site over a complete tidal cycle. An abundant sediment supply and limited resuspension of the bed sediments meant that advection was the main transport process. Our results also demonstrate that detailed analyses of transport processes provide useful information on the sources and fates of suspended sediments, and support the interpretation of morphological changes in accretional intertidal mudflats.

Key words**:** Suspended sediment concentration; resuspension; deposition; advection; bed-level changes; intertidal mudflat

1. Introduction

Suspended sediment concentrations (SSCs) have a major influence on water quality and play an important role in shaping the geomorphology and ecology of estuarine and intertidal wetlands (e.g., Dyer, 1997; Zheng et al., 2004; Schoellhamer et al., 2007; Li et al., 2012). Suspended sediments can transport trace metals, nutrients, organic carbon, and anthropogenic contaminants through estuarine and coastal waters. Furthermore, suspended sediments limit the amount of light entering the water, thereby influencing primary productivity (Tian et al., 2009) and geochemical cycling (e.g., Li et al., 2012). Therefore, to understand the sources and fates of sediments and their associated contaminants, as well as the morphological evolution of intertidal wetlands in detail, the factors that contribute to the variability in SSCs in estuarine and coastal waters should be identified.

Suspended sediment concentrations vary locally in response to three main processes: resuspension and deposition in the vertical direction, and advection in the horizontal direction (e.g., Weeks et al., 1993; Velegrakis et al., 1997; Jago and Jones, 1998; van de Kreeke and Hibma, 2005; Jago et al., 2006; Andersen et al., 2007; Krivtsov et al., 2008; Salehi and Strom, 2012; Yu et al., 2012). The effect of horizontal diffusion is generally neglected because horizontal concentration gradients in macrotidal coastal waters are much weaker than vertical gradients (e.g., Bass et al., 2002; Stanev et al., 2007). Studies of sediment sources have indicated that resuspension processes can cause increases in SSC (e.g., Velegrakis et al., 1997; Christie et al., 1999; Andersen et al., 2007; Salehi and Strom, 2012; Wang et al., 2012; Zhu et al., 2014), whereas deposition processes can cause reductions in SSC (e.g., Dyer, 1989; Salehi and Strom, 2012). Although these studies have indeed provided a qualitative understanding of the causes of variability in SSCs, they generally quantified erosion, deposition and advection processes using at least two observation sites along the main current direction based on suspended sediment transport equation in tidally-dominated coastal environments (e.g., Fugate and Friedrichs, 2002; Yu et al., 2012). However, few studies have quantitatively estimated the relative contributions of erosion, deposition, and advection to SSC variability using a single observation site. In particular, there are few estimates of the transport processes in shallow intertidal environment where waves dominate the hydrodynamic energy. Furthermore, it is indeed easily understood for us that coastal transport processes are advection dominated, but in shallow intertidal environment, vertical turbulent mixing may be large compared with advective transport due to wave action, in other word, bottom sediment resuspension may be responsible for SSC variability (e.g., Anderson, 1972; Janssen-Stelder, 2000; Le Hir et al., 2000; Green, 2011; Wang et al., 2012). Actually, this lack of information in shallow-water environments may reflect the difficulties in working on intertidal wetlands, which are usually composed of very soft, fine-grained sediment and have complex geomorphologies, especially compared with sandy beaches (Wang et al., 2006, 2012; Shi et al., 2012, 2014). In addition, suitable equipment for collecting high-resolution measurements of intratidal bed-level changes during the transport and deposition phases has only recently become available. Therefore, much attention has been directed towards separating the relative contributions of resuspension, deposition, and advection processes from SSC time series, which has generally been performed using numerical models (e.g., Weeks et al., 1993; Jago and Jones, 1998; Ellis et al., 2004; Krivtsov et al., 2008; Yu et al., 2012). However, there is a lack of high-quality data describing transport processes, meaning that the models are oversimplified versions of reality and some of the simplifications and assumptions do not have a sound physical basis. For example, modeling studies have usually either neglected or oversimplified the complex physical processes that play important roles in SSC variability, such as residual and M4 tidal currents, or variations in water depth (Stanev et al., 2007; Cheng and Wilson, 2008).

The physical processes that influence SSC variability have been the subject of discussion for many decades. Some researchers have inferred that an increase in the SSC is only caused by resuspension by high flow velocities or strong waves (e.g., Christie et al., 1999; Janssen-Stelder, 2000; Wang et al., 2012). This inference was made without synchronous *in situ* measurements of intratidal bed-level changes. Other researchers assumed that sudden increases in SSCs were caused by nonlocal erosion and were attributable, in some cases, to advection alone (e.g., Dyer, 1989; Andersen et al., 2007; Salehi and Strom, 2012). For example, Andersen et al. (2007) found that a sudden increase in SSC when the tide was in the ebb phase occurred without bed erosion, suggesting that the increase was entirely attributable to advection (note that this conclusion was made using *in situ* synchronous measurements of intratidal bed-level changes). Hence, it is reasonable to believe that variability in SSC should be attributed not only to resuspension and deposition processes, but also to advection (e.g., Dyer, 1989; Andersen et al., 2007; Salehi and Strom, 2012; Shi et al., 2015). The above evidence suggests that field measurements of intratidal bed-level changes are important in identifying the causes of the variability in SSC (e.g., Dyer, 1989; Andersen et al., 2007; Salehi and Strom, 2012). With the development of high-precision instruments, such as acoustic Doppler velocimeters (ADV; e.g., Andersen et al., 2007; Pratolongo et al., 2010; Salehi and Strom, 2012; Wang et al., 2014; Shi et al., 2015) and acoustic scour monitors (ARXII; e.g., Christie et al., 1999, 2000), which can measure intratidal bed-level changes during submergence and through the transport and deposition phases, it is possible to determine whether an increase in the SSC is caused by resuspension or advection processes over an intertidal wetland. These new technologies also allow the relative contributions of resuspension, deposition, and advection processes to SSCs to be quantified.

The aim of the present study was to investigate the percentage contributions of resuspension, deposition, and advection processes to SSCs in the water column on a highly turbid macrotidal coastal mudflat by monitoring the real-time changes in velocity, water depth, wave height, SSC, and intratidal bed-level. This aim included three specific objectives. First, to quantify the amount of sediment that was resuspended and deposited from *in situ* measurements of the intratidal bed-level changes, and to quantify advection from integrated measurements of the current velocity, depth-averaged SSC, and water depth. Second, to determine the relative contributions of resuspension, deposition, and advection to the SSC in the water column. Finally, to examine the influence of hydrodynamic and environmental factors on the variability in SSC, to extend our understanding of the key controlling variables, and to explain the variability in the contributions from the three transport processes to SSCs. Our results provide new insight into the sources, transport, and fates of sediments. The sediment transport patterns observed in this study have important implications for morphological changes on intertidal mudflats, particularly for accretional intertidal mudflats.

2. Study area

The study area was an exposed mudflat that is part of the larger Wanggang mudflat on the Jiangsu Coast, China, between the abandoned Yellow River Delta and the Yangtze River Estuary (Fig. 1A). The investigated mudflat faces the largest radial tidal sand ridges on the Chinese continental shelf and is northwest of an offshore sand ridge system in the southwestern part of the Yellow Sea (Fig. 1B). The study site is described as a continuous accretional intertidal mudflat because the SSCs over the sand ridge are high (0.2 kg/m^3 on average) throughout the year as a result of the abundant sediment supply provided by the radial tidal ridge system off the Jiangsu coast, the Changjiang River, and the abandoned Yellow River delta (e.g., Ren, 1986; Zhang, 1992; Xing et al., 2012). The values for SSC vary in the range of 0.2–3.0 kg/m^3 on the lower intertidal flat and 0.8–1.6 kg/m^3 on the middle tidal flat (Wang et al., 2012).

The study area is characterized by a macrotidal environment with spring tidal range of between 3.9 and 5.5 m and is dominated by semidiurnal tides (Ren et al., 1985; Ren, 1986; Wang and Ke, 1997; Wang et al., 2012; Xing et al., 2012). It is a well-developed mudflat with a slope of only 0.018%–0.022% and a maximum width of 25 km (Liu et al., 2013); the width typically ranges from several kilometers to tens of kilometers (e.g., Zhu et al., 1986; Wang and Ke, 1997). There is a gauging station on the middle mudflat, approximately 6 km seaward from the sea wall (Fig. 1B), and there are no distinct creeks near the station. The surficial sediments are mainly silt and fine sand (Wang and Ke, 1997). During our field measurements, the median grain size of the bottom sediments in the uppermost 1–2 cm layer ranged from 68.1 to 75.7 μm. The bottom sediments were composed of grains of >63 μm (from medium to very fine sand) and <63 μm (silt and clay) (Fig. 2).

3. Methods

3.1 Field measurements

The field measurements were made after the instruments were secured to a custom-made tripod. The tripod had been tested on previous occasions, and is an open structure with three stainless-steel legs, anchored at least 1.5 m deep in the bed to maintain its stability. The measurements of water depth, wave height, turbidity, near-bed boundary velocities, and intratidal bed-level changes were recorded synchronously from 27 to 30 April, 2013.

Water depth and wave height were measured with a wave–tide recorder (SBE 26plus SEAGAUGE Wave and Tide Recorders, Sea-Bird Electronics, USA). This instrument (Resolution: 0.4 mm for wave measurement; Measurement accuracy: 0.01% of the full scale) consists of a pressure sensor that was placed horizontally on the bed, close to the tripod, at a height of 0.15 m above the sediment surface. The sensor recorded data at a frequency of 4 Hz over a 256 s period, giving a total of 1024 measurements per burst. The water depth and significant wave height were calculated according to the manufacturer's software. To obtain a complete curve of the water depth, the distance between the pressure sensor and the sediment surface was corrected by adding 0.15 m to all the measured water depths to accommodate the distance between the pressure sensor and the sediment surface.

Turbidity, salinity, and temperature were measured using three optical backscattering sensors on a self-recording instrument (OBS-3A Turbidity and Temperature Monitoring System; Washington, USA). The backscattering sensors (measurement accuracy: ±0.1 NTU (0-100 NTU), ±1 NTU (100-500 NTU), ±5 NTU (500-4000 NTU); sampling rate: 8 Hz) were positioned with their sensors facing outward at heights of 10, 20, and 40 cm above the bed. Unfortunately, the turbidity data at heights of 20 and 40 cm above the surface are missing for Tide 1 (27 April 2013) because of instrument failure. *In situ* water samples collected from a boat during the collection of field measurements were used to calibrate the turbidity measurements and to estimate the errors associated with the SSC estimates from the optical backscattering sensors.

The current velocity profiles were measured using an acoustic Doppler profiler (ADP-XR, SonTek, USA) with a sampling interval of 5 min. The ADP-XR (measurement accuracy: ±1% of measured velocity; velocity resolution: 0.1 cm/s; blanking distance: 20 cm) was mounted on the seabed with the sensor probe facing upwards, at 5 cm above the sediment surface. The near-bed boundary velocities and intratidal bed-level changes were recorded using a 6 MHz Nortek Vector ADV (acoustic transmitter; measurement accuracy: ±1 mm/s; sampling rate of 1-64 Hz) orientated downward, with its sensor installed 20 cm above the bed (i.e., the same height as the optical backscattering sensors). Data were collected in burst mode at 2 min intervals (sampling time). The ADV also recorded the distance from the probe to the surface of the sediment (i.e., the boundary elevation; Salehi and Strom, 2012; measurement accuracy: ±1 mm). The vertical distance from the probe to the surface of the sediment increases when resuspension occurs (net erosion), and decreases when deposition occurs (net accretion) (Salehi and Strom, 2012; Wang et al., 2014). Thus, changes in the bed level attributable to net erosion or accretion can be measured using the ADV. We thus acquired information on the intratidal bed-level changes during the data collection periods, and related erosion and deposition from the time series (Andersen et al., 2007; Salehi and Strom, 2012; Wang et al., 2014). We used an ADV because it can provide data on intratidal bed-level changes to an accuracy of 1 mm (Andersen et al., 2007; Salehi and Strom, 2012). The accuracy of the bed-level measurements made with the ADV has been tested in the laboratory (Salehi and Strom, 2012) and in the field (Andersen et al., 2007). The ADV can provide co-located, simultaneous measurements of current velocity and changes in bed elevation. It can also measure bed-level changes and current velocities in very shallow water because the sampling distance is just 15 cm from the probe head. Accurate measurements are important to ensure robust quantitative estimates of the contributions of resuspension and deposition to SSCs. After the ebb time, we sampled bottom sediments over an area of 0.2 × 0.2 m at a depth of 0.05 m to determine the mass and density of wet and dry sediment. Surface sediment was collected from the uppermost 1–2 cm for grain size determination.

3.2 Sample analysis and data processing

3.2.1 Sediment sample analysis

On arrival at the laboratory, the wet bottom sediments were weighed (M_{wet}), dried at 50°C until constant weight was achieved (~2 days), and then weighed again (M_{dry}). The ratio of wet to dry sediment mass was defined as β (β = M_{wet}/M_{dry}). Following Shi et al. (2012), the surface sediment samples were deflocculated before grain size determination to avoid measuring any larger flocs. The grain size was measured using a laser particle size analyzer (LS13320, Coulter, USA).

3.2.2 Calculation of shear stresses

The shear stress generated by waves (τ_w) is closely related to the wave orbital velocity ($\hat{U}_\delta$, m/s, Eq.1) at the edge of the wave boundary layer, and $\hat{U}_\delta$ is given by wave parameters (wave height, wave period and water depth) (Whitehouse et al., 2000; Zhu et al., 2014) derived from wave measurement using SBE 26plus SEAGAUGE :

$$\hat{U}_\delta = \frac{\pi H}{T \sinh(kh)} \quad (1)$$

where H is wave height (m), T wave period (s), h water depth (m), k (= $2\pi/L$) the wave number, L[= $(gT^2/2\pi)$ tanh(kh)] the wavelength (m), and g the gravitational acceleration (=9.8 m/s^2).

The shear stress τ_w can then be calculated as follows (van Rijn, 1993):

$$\tau_w = \frac{1}{2} \rho_w f_{wr} \hat{U}_\delta^{\,2} \tag{2}$$

where ρ_w is seawater density (=1030 kg/m^3), f_{wr} wave friction coefficient calculated by an equation provided by Soulsby (1997), utilizing the equivalent bed roughness k_s = 25 η^2/λ (Davies and Thorne, 2005) because the ripples were present at the present study areas. The parameters η and λ are the ripple height and the ripple wavelength, respectively, and are obtained by the *in situ* measurements of bed ripples.

The turbulence velocity from ADV can be decomposed into two terms: the mean and fluctuating components (i.e., u = ū + ú, u denotes the measured velocity, ū the mean velocity, and ú the mean turbulence velocity). Therefore, the Turbulent Kinetic Energy (TKE) can be estimated from the turbulent fluctuations (Eq.3) (Andersen et al., 2007; Shi et al., 2015), and then the shear stress generated by the current (τ_c) is expressed by Eq.4.

$$E_{TKE} = \left(u'^2 + v'^2 + w'^2\right)/2 \tag{3}$$

$$\tau_c = C\, E_{TKE} \tag{4}$$

where E_{TKE} is the Turbulent Kinetic Energy (TKE), u', v' and w' are the time-varying fluctuating velocity components, C a constant (=0.19, Stapleton and Huntley, 1995; Kim et al., 2000; Pope et al., 2006).

In the van Rijn (1993) model, the bed shear stress generated by combined current-wave action (τ_{cw}, N/m^2) can be calculated by current-wave model (Eq.5) proposed by van Rijn (1993).

$$|\tau_{cw}| = \alpha_r \ \tau_c + |\tau_w| \quad (5)$$

$$\alpha_r = \left[\frac{\ln(30\,\delta/k_a)}{\ln(30\delta/k_s)}\right]^2 \left[\frac{-1+\ln(30h/k_s)}{-1+\ln(30h/k_a)}\right]^2 \quad (6)$$

where k_a is the apparent bed roughness, and k_s the bed roughness. Based on the recommendation of van Rijn (1993), k_a equals k_s (i.e., $\alpha_r = 1$) when the ratio of the peak orbital velocity to depth-averaged velocity is 1. The value for τ_c is positive when the wave direction is the same as the current direction, whereas is negative when the wave direction is opposite to the current direction (van Rijn, 1993).

Sediment samples from the Wanggang mudflat (the present study area) showed no obvious biological community structure. The samples consist of sediments with less than several tens of microns and high water content. The median grain sizes of bottom sediments were 68.1–75.7 μm, and the sediment water content was 31% at the observation site. Based on recommendation of Taki (2000), we determined the critical shear stress for erosion (τ_{cr}, N/m^2) using Eq.7.

$$\tau_{cr} = 0.05 + \gamma \left\{ \frac{1}{\left[\left(\pi/6\right)\left(1+sW\right)\right]^{1/3} - 1} \right\}^2 \quad (7)$$

where W is the sediment water content (measured in the laboratory); the dimensionless coefficient γ was chosen to be 0.3 based on the experimental data of Taki (2001); s (=ρ_s/ρ_w -1) the specific weight of a particle; ρ_s (=2650 kg/m^3) the sediment particle density, ρ_w seawater density (=1030 kg/m^3, measured in the laboratory).

3.2.3 Erosion (E) flux and deposition (D) flux

The intratidal bed-level change data recorded with the ADV were used to calculate the wet sediment mass per unit horizontal area per unit time produced by erosion ($M_{wet\text{-}E}$) and deposition ($M_{wet\text{-}D}$), and further $M_{wet\text{-}E}$ and $M_{wet\text{-}D}$ were converted into erosion flux and deposition flux, respectively. Thus the $M_{wet\text{-}E}$ and $M_{wet\text{-}D}$ were estimated as follows:

$$M_{wet\text{-}E} = (D_{i+1} - D_i) \times \rho_{wet} \times (1/\text{Interval}) \qquad D_{i+1} > D_i \qquad (8)$$

$$M_{wet\text{-}D} = \left| D_{i+1} - D_i \right| \times \rho_{wet} \times (1/\text{Interval}) \qquad D_{i+1} < D_i \qquad (9)$$

where ρ_{wet} is the density of the wet sediment (kg/m^3), D is the distance from the probe to the surface sediment recorded with the ADV, and i is part of the bed elevation time series. In other words, the value of D_{i+1} is greater than the value of D_i when erosion occurs, but less when deposition occurs. Interval is 120 s based on setup of ADV in the Section 3.1. In this study, the unit of $M_{wet\text{-}E}$ and $M_{wet\text{-}D}$ should be kg/m^2/s on the basis of Eq. 8 and 9.

The sediment flux produced by erosion (E, kg/m^2/s) and deposition (D, kg/m^2/s) was calculated as follows:

$$E = M_{wet\text{-}E}/\beta \qquad (10)$$

$$D = M_{wet\text{-}D}/\beta \qquad (11)$$

where β is the wet to dry sediment mass ratio (i.e., β is the ratio of wet to dry sediment mass), and is defined in the Section 3.2. These wet mass estimates above based on *in situ* ADV measurements of intratidal bed-level changes, can be converted into erosion flux or deposition fluxes (dry mass per unit area per unit time; kg/m^2/s) based on Eq.10 and 11.

On the other hand, theoretically, the erosion flux E is related to erodibility contant, τ_{cw} and τ_{cr}, and could be predicted using these parameters, and is expressed as Eq.12 (e.g., Johnsen et al., 1994; Winterwerp and van Kesteren, 2004; Lumborg, 2005; Zhu et al., 2014):

$$E = M\,[(\tau_{cw}/\tau_{cr}) - 1] \quad \text{for} \quad \tau_{cw} > \tau_{cr} \qquad (12)$$

where E is the erosion flux (kg/m^2/s), τ_{cw} is the bed shear stress generated by combined current-wave action (N/m^2), τ_{cr} is the critical bed shear stress for erosion (N/m^2), M is erodibility contant (kg/m^2/s), and the applied value of M in this study was 0.1 kg/m^2/s based on recommendation provided by Shi et al.(2014) and Zhu et al.(2014), which is on the same order of magnitude as a large number of published results (e.g., Johnsen et al., 1994; Whitehouse et al., 2000; Winterwerp and Van Kesteren, 2004; Lumborg, 2005).

The deposition flux D, theoretically, is depended on settling velocity (w_s) of suspended sediments and SSC in the tidal water, and generally is expressed by Eq.13 (Winterwerp and van Kesteren, 2004):

$$D = w_s c_b\,[1-(\tau_{cw}/\tau_{cd})] \quad \text{for} \quad \tau_{cw} < \tau_{cd} \qquad (13)$$

where D is the deposition flux (kg/m^2/s), w_s is median settling velocity of the sediments (m/s), c_b is the near-bed suspended sediment concentration (SSC, kg/m^3), and τ_{cd} is critical shear stress for the deposition of suspended sediment (e.g., Krone 1962, van Rijn 1993, Soulsby 1997, Shi et al., 2012). The τ_{cd} ranges from 0.01 to 0.1 N/m^2, and is typically 0.05 N/m^2 for fine-grained sediment (Lumborg, 2005). Therefore, the applied value of τ_{cd} is 0.05 N/m^2 in the present study because the suspended sediments in the present intertidal wetland are composed of a range of fine-grained mineral particles (Fig.2).

A strong correlation is found between SSC of water samples and turbidities (SSC=0.0031T, correlation coefficient R^2 is 0.97, T denotes turbidity). In this study, near-bed turbidities measured by OBS-3A in the field can be converted to SSC using this calibrated regression equation.

3.2.4 Suspended sediment flux

To obtain accurate estimates of SSC in the water column, the turbidity measurements recorded in the field by the three optical backscattering sensors were calibrated using *in situ* water samples, following Yang et al. (2007). The relationships between turbidity (T, measured in nephelometric turbidity units, NTU) and SSC (kg/m^3) were expressed as follows:

SSC = 0.0019T + 0.06 (R^2 = 0.98), mean relative error = 0.018 (10 cm above the bed),

SSC = 0.0008T + 0.44 (R^2 = 0.81), mean relative error = 0.116 (20 cm above the bed),

SSC = 0.0018T + 0.09 (R^2 = 0.98), mean relative error = 0.016 (40 cm above the bed),

where R^2 is the correlation coefficient for the fitted relationship, and the mean relative error represents the error between the measured and calibrated SSCs.

Using these calibrated SSC values, suspended sediment flux (*F*, dry suspended sediment mass per unit area per unit time, $kg/m^2/s$) is expressed as follows:

$$F = \frac{1}{H}\int_{H} \mathrm{SSC}(z, t)\, u(z, t)\, dz \quad (14)$$

where H is water depth (m), z is height (m) above the bed, t is time (s), and u is mean current velocity (m/s).

3.2.5 Percentage contributions of resuspension, deposition, and advection to SSC in the water column

Using the above information, we can calculate the percentage contributions of erosion and deposition to SSC with Eq.15 and Eq.16, respectively:

$$\varphi_E = 100\% \times E/F \tag{15}$$

$$\varphi_D = -100\% \times D/F \tag{16}$$

where φ_E and φ_D are the percentage contributions of resuspension and deposition to the SSC in the water column, respectively. In this study, φ_E is positive when resuspension causes an increase in the SSC, and φ_D is negative when deposition causes a reduction in the SSC. To show clearly relationship between suspended sediment flux(F), erosion/deposition(E/D) flux and advective flux (F_0), we have given a conceptual diagram in term of their relationships (Fig.3).

On the basis of φ_E and φ_D, the percentage contribution of advection (φ_A) to SSC can be calculated as follows:

$$\varphi_A = (1 - \varphi_E) \times 100\% \qquad D_{i+1} > D_i \tag{17}$$

$$\varphi_A = (1 - \varphi_D) \times 100\% \qquad D_{i+1} < D_i \tag{18}$$

3.3 Empirical orthogonal function (EOF) analysis

The empirical orthogonal (eigen) function (EOF) is a powerful analytical technique for extracting detailed information from large datasets. The technique has been widely applied in studies of sediment transport, morphological change, and suspended sediment dynamics (e.g., Liu and Lin, 2004; Liu et al., 2009; Dai et al., 2010, 2013a, 2013b). The technique breaks down a set of intercorrelated variables into a small number of statistically independent variables (Dai et al., 2013a, 2013b). In this study, the values for possible influential factors (water depth, salinity, water temperature, current velocity [U_b], significant wave height [H_s], wind speed, and SSC), as collected during the field campaign, were standardized to form a single matrix M:

$$M = M(M_1 \ldots M_m) \tag{19}$$

where M is an n × m matrix, *n* represents a potential control on the variability of the SSC, and m is the observed time.

A standardized covariance matrix S (S = M M′) was then produced (matrix M′ is the transpose of matrix M). Matrix S was then broken down to obtain the eigenvalues $\lambda(\lambda_1 \ldots, \lambda_m)$ and the influencing factor modes (V). The cumulative contribution (Φ) of the first *k* eigenvalues of matrix S was calculated as follows (e.g., Dai et al., 2013a):

$$\phi = \sum_{i=1}^{k} \lambda_i \Big/ \sum_{i=1}^{m} \lambda_i \tag{20}$$

The cumulative contribution represents the main information from the original datasets when Φ > 85% (Emery and Thomson, 2001; Dai et al., 2013b).

4. Results

4.1 Wind speed, water depth, and current velocity

We split the analysis into two periods representing calm weather (Tides 1–4 and 6) and rough weather (Tide 5). The analysis of wind speed measured at Dafeng Harbor indicated that the calm weather conditions were characterized by wind speeds of 3.2–9.8 m/s and an average wind speed of 7.4 m/s. The wind was in an offshore direction (131°–170°) during Tides 1–4, and in an onshore direction (30°–115°)

during Tide 6 (Fig. 4C). In contrast, the rough weather conditions were characterized by an onshore wind (0°–26°) with maximum and average speeds of 13.9 m/s and 9.2 m/s, respectively (Fig. 4C).

The observed changes in water depth are shown in Fig. 4A and Table 1. The maximum water depth for six consecutive tides ranged from 0.77 to 1.50 m, and the mean water depth ranged from 0.64 to 1.10 m (Table 1). The duration of submergence was 4.0–4.5 h, with different durations for flood and ebb phases, indicating that the tide was asymmetrical during the period of field measurements (Fig. 4A).

For the entire study period, the current velocity varied from 0.10 to 0.65 m/s (Fig. 4B; Table 1). The average current velocity was greater during the ebb phase than during the flooding phase (Fig. 4B). The current velocity rotated in a clockwise direction, and tended to be onshore (southwestward) during the initial stages of flooding, alongshore (northwestward) during the middle and high tides, and offshore (northeastward) during the ebb stage (Fig.4B). The current reached a maximum velocity in the offshore direction around the middle stage of the ebb phase (Fig. 4B).

4.2 Wave height, salinity, and water temperature

During calm weather, the maximum and average wave heights were 0.08–0.25 m and 0.06–0.13 m, respectively. In contrast, during rough weather the maximum and average wave heights were 0.38 and 0.2 m (Table 1), respectively, showing that wind had a significant influence on wave height.

Time series for tidal water salinity and temperature are shown in Fig. 5B. The water salinity, measured in practical salinity units (PSU), ranged from 22 to 25 (Table

1) and was slightly lower during the flood phase than during the ebb phase (Fig. 5B).

4.3 SSC and bed-level changes

The values of SSC (z = 10 cm) near the bed (ranged from 0.5 to 2.8 kg/m^3) were noticeably higher than those measured at 20 and 40 cm above the bed (ranged from 0.2 to 1.5 kg/m^3) during normal weather, although the values for all three heights showed similar temporal fluctuations (Fig.5C). The average SSCs during rough weather conditions were higher than those at corresponding heights during calmer weather (Table 1).

The time series of intratidal bed-level changes is shown in Fig.5D. Negative values denote erosion, and positive values denote deposition. Although there was a general trend of accretion in the bed level during Tides 1–4 and Tide 6, and erosion during Tide 5, erosion and deposition fluctuated frequently (Fig. 5D). Strong erosion occurred during rough weather, and the maximum erosion rate was –0.26 mm/s. In contrast, the maximum deposition rate of +0.13 mm/s was measured during calm weather.

4.4 Bed shear stresses

The bed shear stresses due to currents (τ_c), waves (τ_w) and combined current–wave action (τ_{cw}), are shown in Fig.6B, C and D. The maximum and average values of τ_c were 0.048–0.224 N/m^2 and 0.021–0.093 N/m^2 (Tide 2) during the field measurements. The value of τ_w was relatively stable during Tides 1–4 (0.022–0.056 N/m^2 on average), and was smaller than the corresponding τ_c during Tides 1–4 and 6–10. The τ_w increased dramatically during Tide 5 (average = 0.10 N/m^2 for Tide 5).

The τ_{cw} was calculated using the model of van Rijn (1993). For the total tide, the average value of τ_{cw} was 0.025–0.122 N/m^2. The maximum values of τ_{cw} during the field measurements occurred on Tide 5 and were 0.292 N/m^2.

4.5 Sediment fluxes

The estimated values for *E*, *D*, and *F* are listed in Table 2 and shown in Fig.5E. The value for *E* was greater during Tide 5 than during Tides 1–4. The average value for *F* (1.02 kg/m^2/s) during Tide 5 were greater than the values for *E* (0.02 kg/m^2/s) and *D* (0.02 kg/m^2/s) for corresponding tide (Table 2), and the average value for *F* (ranged from 0.13 to 0.32 kg/m^2/s) during Tide 1-4 and 6 were greater than the values for *E* (ranged from 0.01 to 0.02 kg/m^2/s) and *D* (ranged from 0.01 to 0.02 kg/m^2/s) for corresponding tide. In all, from Table 2, on average advection flux was at least 9.5 times higher than erosion flux (*E*) and deposition flux (*D*) of corresponding tide.

Erosion flux and deposition flux inferred from *in situ* bed-level changes and predicted by engineering formula, respectively, was showed in Fig.6*E* and *F*. For erosion flux (Fig.6*E*), the values of erosion flux inferred from *in situ* bed-level changes (ranged from 0.002 to 0.043 kg/m^2/s) are same order of magnitude as that predicted by engineering formula (ranged from 0.001 to 0.059 kg/m^2/s). For deposition flux (Fig.6F), the values of deposition flux inferred from *in situ* bed-level changes (ranged from 0.001 to 0.041 kg/m^2/s) are also same order of magnitude as that predicted by engineering formula (ranged from 0.001 to 0.042 kg/m^2/s). Overall, this study could provide an important hint for understanding sediment dynamic processes in the rough turbulent boundary layers.

4.6 Percentage contributions of resuspension, deposition, and advection processes

The percentage contributions of resuspension (φ_E), deposition (φ_D), and advection (φ_A) to the SSC in the water column are shown in Fig.5F and listed in Table 2. Over the entire period of field measurements, the maximum values for φ_E and φ_D ranged from 9.07% to 41.32% and from –8.24% to –34.27%, respectively (the minus sign denotes a negative contribution to the SSC) (Table 2). On average, the absolute value for φ_E was similar to that for φ_D. In contrast, the average value for φ_A was much larger than the absolute values for φ_E and φ_D for a corresponding tide (Fig.5F), showing that advection was the main cause of the variation in SSC. The contributions of resuspension and deposition were minor in comparison.

4.7 EOF analysis

Advection, resuspension, and deposition processes are determined by hydrodynamic conditions (e.g., water depth, wind, current velocity [U_b], and wave height [H_s]) (e.g., Andersen et al., 2007; Wang et al., 2006, 2012; Zhu et al., 2014), and are influenced by environmental factors such as water temperature and salinity (e.g., Krögel and Flemming, 1998; Xing et al., 2010, 2012). Salinity is also a key indicator of net water movement onshore/offshore. Therefore, datasets of the hydrodynamic and environmental factors and SSC during each tidal cycle were analyzed with EOF to identify the major modes of correlated variance. The first three modes explained 84.8%–92.0% of the correlations (standardized covariance) (Fig.6). The eigenvectors show the groupings of the variables in the data set, and the eigenweights indicate the temporal distributions of the variables. The most important mode (mode 1) explained 36.4%–62.4% of the data, and showed an inverse relationship between salinity and SSC (Fig.7A2–C2, E2–F2), a positive correlation between salinity and temperature during the daytime (Fig. 7A2, C2), and an inverse relationship between salinity and temperature at night (Fig.7B1, D1, F1). The mode for Tides 1–3 describes the increase in salinity and hydrodynamics, and the associated reduction in SSC during the tidal cycle (Fig.7A2–C2). This mode indicates that high SSC occurred in less-saline water under flood conditions and that SSC correlated weakly with the hydrodynamic conditions. Conversely, this mode for Tide 5 shows that the current velocity, wave height, and SSC reached their maxima in high water (Fig. 7E1). The second mode accounted for 21.1%–32.6% of the correlations (Fig. 7). The grouped variables indicate that waves were responsible for most of the variability in SSC in Tides 3, 5, and 6 (Fig. 7C2, E2, and F2). Because the third mode of Tides 1, 2, 3, and 6 explained less than 10% of the data, only Tides 4 and 5 (explaining 11.7% and 15.8% of the data, respectively) are described (Fig. 7). This mode shows that SSC variability correlated positively with wind speed and waves in Tide 4, and with wind speed in Tide 5 (Fig. 7D1–E1).

5. Discussion

5.1 Contributions of erosion, deposition, and advection to SSC variability

Erosion flux and deposition flux are important and fundamental sedimentary processes, and are key concepts for quantifying intertidal morphological behavior and sediment transport in the aquatic environment. A large number of studies have conducted many laboratory or field experiments for assessing erosion and deposition event (e.g., Partheniades, 1965; Ariathurai and Krone, 1976; Dyer, 1986; Mehta, 1988; Mehta et al., 1989; Van Leussen and Winterwerp, 1990; Sanford and Halka, 1993; Janssen-Stelder, 2000; Winterwerp and van Kesteren, 2004; Andersen et al., 2007; Shi et al., 2012; Zhu et al., 2014), and thus many engineering formulas for predicting sediment erosion flux or deposition flux have been produced (e.g., Partheniades, 1962, 1965, 1986, 1993; Johnsen et al., 1994; Winterwerp and van Kesteren, 2004; Lumborg, 2005). However, to date, there has still disputed in term of physical meaning of erosion flux and deposition flux in the scientific community. First, erosion flux and deposition flux are considered dividually, and erosion event occurs only when $\tau_{cw} > \tau_{cr}$ (Eq.12), and deposition event occurs only when $\tau_{cw} < \tau_{cd}$ (Eq.13) (e.g., Whitehouse et al., 2000; Lumborg, 2005; Shi et al., 2012). Second, erosion and deposition event occur simultaneously, and net erosion occurs only when $E > D$, and net deposition occurs only when $D>E$ (e.g., Ariathurai and Krone, 1976; Dyer, 1986; Mehta, 1988; Mehta et al., 1989; Van Leussen and Winterwerp, 1990; Sanford and Halka, 1993; Winterwerp and van Kesteren, 2004; Shi et al., 2014). Therefore, two assumptions above should be tested further. In the present study, we have predicted E and D based on τ_{cw}, τ_{cr}, τ_{cd} and SSC (Eq.12 and 13), and have also inferred E and D from *in situ* measurement of intratidal bed-level changes from ADV(Fig.6). The present results showed that theoretically this prediction and inferring of E and D appears to support the first assumption, in other words, erosion and deposition event can not occur simultaneously. In fact, this assumption was also supported by many erosional and depositional flume or field experiments (Partheniades, 1965; Sanford and Halka, 1993;

Winterwerp and van Kesteren, 2004; Shi et al., 2012; Zhu et al., 2014). For example, Partheniades (1965) carried out three experiments in a rotating annular flume, suggesting that deposition and erosion cannot occur simultaneously in the rough turbulent boundary layers. Therefore, an analysis from field and theoretical investigation of erosion flux and deposition flux is an important implication in understanding erosional and depositional mechanisms that underlie the sedimentary process and morphological evolution in intertidal wetland environments.

In this study, the value of τ_c during Tides 1–4 was comparable with the value of τ_c at the flooding stage of Tide 5 (Fig.6C), whereas the value of τ_w at the flooding stage of Tide 5 was greater than that during Tides 1–4 (Fig. 5B), and severe erosion occurred only during Tide 5 (Fig.5D), suggesting the importance of waves to the dynamic processes associated with sedimentation in the intertidal environments, and that local intratidal sediment suspension and sedimentation can be dominated by wave action. This is probably the case for other intertidal mudflats. For example, Janssen-Stelder (2000) found that during calm weather, deposition occurred and current velocities were the dominant processes, whereas during storms, erosion occurred and wave activity dominated, indicating that variations in hydrodynamic conditions have a direct effect on erosion or accretion on tidal flats and that the role of waves in resuspending bottom sediments is also of importance.

The present analysis of the percentage contributions of erosion, deposition, and advection processes shows that on average advection flux was at least 9.5 times higher than erosion flux and deposition flux of corresponding tide (Table 2). Thus the variability in SSC was mainly controlled by advection, with only limited contributions from erosion and deposition event (Fig. 5F). Theoretically, the variability of SSC at a given location is governed by the mass conservation equation, and sediment erosion and accretion on the tidal flat depends on spatial gradient of advection flux (e.g., Weeks et al., 1993; Bass et al., 2002; Yu et al., 2012). Previous studies in this area have reported that for a complete tidal cycle, the depth-averaged SSC over the lower intertidal flat (peak SSC >3 kg/m^3) is generally higher than that over the middle intertidal flat (0.8–1.6 kg/m^3) during normal weather (Wang et al., 2012), and there has abundant sediment supply from the radial tidal ridge system located between the Yangtze River and the abandoned Yellow River Delta (Ren, 1986; Zhang, 1992; Wang et al., 2006; Wang et al., 2012; Xing et al., 2012). Whereas depth-averaged SSC ranged from 0.66 to 1.5 kg/m^3 during calm weather in this study, and the present observation site was also located at the middle intertidal flat. Therefore, It is reasonable that in this study the variability in SSC is mainly controlled by advection owing to spatial gradient of advection flux from lower intertidal flat to the middle intertidal flat based on advective diffusion equation. This case also appears in the other estuarine systems. For example, Velegrakis et al. (1997) found that the SSC variability was mainly controlled by advection along a cross-section of the central English Channel, which they attributed to the same causes as those identified in the present study. They found that large quantities of sediments derived from the coastal zone and estuarine environments with high SSC were advected towards the offshore waters of the English Channel, where the SSC was very low, and that the high SSC in the bottom layer was unlikely to result from *in situ* sediment erosion, but appeared instead to be controlled mainly by advection due to existence of spatial gradient of advection flux. Additionally, the present case also reflects the limited erosion resulting from long-term consolidation of the bottom sediments. Consolidation takes ~9 h during the between-tide phases at the gauging station. The length of time taken can increase the bed strength and the critical shear stress required for the erosion of bed sediments, resulting in a reduced erosion rate. Whereas the situation reported by Velegrakis et al. (1997) probably reflects the limited contribution of the erosion of bottom sediments to the SSC, as we postulated, because of the bed armoring that prevented the erosion of fine-grained sediments (Velegrakis et al., 1997).

5.2 Influence of dynamic and environmental factors on variability in SSC and implications for morphological changes

Many previous studies of sediment dynamics have shown that hydrodynamic factors (e.g., water depth, wind, current velocity [U_b], and wave height [H_s]) and environmental factors (e.g., water temperature and salinity) may directly influence resuspension, deposition, and advection processes (e.g., Krögel and Flemming, 1998; Wang et al., 2006, 2012; Andersen et al., 2007; Xing et al., 2010, 2012; Shi et al., 2012; Zhu et al., 2014). For example, a reduction in water temperature leads to (1) an increase in water viscosity and the critical shear stress required to erode bottom sediments; (2) a reduction in the settling velocity of sediments (Krögel and Flemming, 1998; Table 5 in Xing et al., 2012); and (3) a reduction in resuspension and deposition (Xing et al., 2012). Sudden increases in wind strength or wave height may cause greater resuspension of the bottom sediments (e.g., Janssen-Stelder, 2000; Andersen et al., 2007; Wang et al., 2012). In contrast, when hydrodynamic conditions are weak, the sediment in the tidal water is unlikely to remain in suspension (e.g., Cancino and Neves, 1999; Christie et al., 1999; Lumborg, 2005; Shi et al., 2012), resulting in greater deposition. Therefore, as well as the processes described above, hydrodynamic and environmental factors can influence erosion, deposition, and advection, and are therefore additional controls on SSC variability.

In this study, we used an EOF analysis to determine the hydrodynamic and environmental factors that exerted most control on the temporal changes in SSC variability on an accretional coastal mudflat. Our results clearly explain why advection had the greatest influence on the variations in SSC. The inverse relationship between SSC and salinity, and the weak correlation between SSC and hydrodynamic conditions indicate that the high suspended sediment load during flood conditions is carried by less-saline water, and that the suspended sediment is not locally sourced, but is derived from elsewhere (less-saline water, high SSC), most likely from the radial sand ridge system. Northwestwardly or southwestwardly flood water from offshore (the radial sand ridge system) arrived at the study site first, transporting less-saline water with a higher SSC. As the water level increased, the hydrodynamics strengthened, and the study site was influenced by more offshore water; salinity increased and SSC decreased until the ebb phase. The EOF results confirm that the sediment transport patterns were dominated by advection, promoted by an abundant sediment supply and the limited resuspension of bed sediments

Advection was probably driven by wind, currents, and related alongshore transport. In the field study, the wind field was northward during Tides 1–4, southward during Tide 5, and westward during Tide 6 (Fig. 4). Conversely, the current turned in a clockwise direction, from southwestward to northward. These prevailing wind and current directions provide a plausible explanation for the advection of the abundant sediment supply from the radial tidal ridge towards our field location, and helps explain why advection was the major factor controlling the variability in SSC. The covariations in SSC and hydrodynamic factors in the less important modes provide further confirmation that suspension plays a minor role in SSC variability.

The pattern of sediment transport described in this study has important implications for morphological changes that occur in intertidal mudflats, especially in accretional intertidal mudflats. We explain these implications in the context of our study site. The gauging station is located in the middle of an intertidal mudflat, and accretion occurs under calm weather conditions (Fig. 5D). Therefore, it is reasonable to expect that weaker hydrodynamic conditions occur on the upper part of this intertidal mudflat because the current and wave energies are attenuated (e.g., Shi et al., 2010, 2012; Yang et al., 2012), resulting in enhanced accretion on the upper intertidal mudflat during calm weather. This proposal was confirmed by the findings of the bed elevation surveys on this intertidal mudflat reported by Wang et al. (2012). Their results show significant accretion of the intertidal profile since 1978 (Fig. 12 in Wang et al., 2012). The maximum accretion thicknesses was 0.18 m, and the accretion rate ranged from ~0.80 to 2.82 mm/day on the upper intertidal mudflat from May to

December 2008 (Fig. 9 in Wang et al., 2012). The observed advection-dominated sediment transport pattern introduces an abundant sediment supply to the upper intertidal mudflat. Therefore, the study area is termed an accretional intertidal mudflat because of this sediment transport pattern.

Although we interpreted the major factors and physical mechanisms controlling the variability in SSC in detail, together with implications for related morphological changes, our research indicates that further studies are required to provide a complete understanding of the sources and fates of suspended sediments on macrotidal mudflats. In particular, further studies should focus on (1) improving the precision of predictions of E and D. Although predicted values of E and D are at least acceptable compared with inferred values of E and D, predicted values are sometime big different with corresponding inferred values; (2) estimating the contributions of resuspension, deposition, and advection to SSC variability during typhoon or storm events, because these conditions are likely to influence their relative contributions; (3) extending our understanding of the factors that control variations in SSC when there is abundant sediment resuspension or a limited sediment supply from estuaries or coastal lagoons; and (4) examining variability in SSC in very-shallow-water environments (e.g., water depths < 10 cm) dominated by waves. Such studies would extend our understanding of the physical processes that control sediment transport, and their role in the morphological changes that occur on intertidal mudflats.

6. Conclusions

We undertook field measurements of intratidal bed-level changes, water depth, wave height, current velocity, and SSC on a highly turbid, accretional macrotidal mudflat on the Jiangsu Coast, China. These measurements were used to quantify the relative roles of erosion, deposition, and advection on SSC variability. The major findings of this study are as follows.

1. Sediment flux estimates for erosion, deposition, and advection demonstrated that average advection flux was much higher than average erosion flux and deposition flux of corresponding tide, and that advection, driven by tidal currents, wind, and associated alongshore transport, was responsible for almost all the variability in SSC over a complete tidal cycle.

2. An EOF analysis of the influence of hydrodynamics and environmental factors on the SSC variability showed that the advection-dominated sediment transport pattern occurred because of an inverse relationship between SSC and salinity, and that SSC and hydrodynamic conditions correlated only weakly. Our results also indicate that the high suspended sediment loads observed during flood conditions were transported by less-saline water, and that the source of this sediment was not, but from elsewhere (a less-saline environment with a high SSC), most likely the radial sand ridge system. Therefore, we conclude that advection is the key transport process because of the abundant sediment supply and the limited resuspension of bed sediments.

3. Analysis of the advection-dominated sediment transport pattern demonstrated

why this particular intertidal mudflat is accretional, and showed that detailed studies of transport processes can help to identify the sources and fates of suspended sediments. These findings help to interpret morphological changes in intertidal mudflats.

Future research on the sources and fates of suspended sediments should focus on estimating the relative contributions of resuspension, deposition, and advection transport processes to SSC variability, particularly under more extreme weather conditions than were studied here (such as typhoon or storm events), and focus on improving our understanding of the variability in SSC in very-shallow-water wave-dominated environments (e.g., water depths < 10 cm), both of which are likely to present different sediment transport patterns.

Acknowledgments

This study was supported by the Major State Basic Research Development Program (2013CB956502), the Natural Science Foundation of China (no. 41376044), the Chinese Geological Survey Project ‘Geological Environment Survey and Assessment on Jiangsu Coastal Economic Zone’ (1212011220005), the Natural Science Foundation of Jiangsu Province (BK20130569), and the PAPD of Jiangsu Higher Education Institutions. We thank Liu Runqi, Wang Yingfei, Yuqian, Zhu Qingguang, Ni Wenfei, Zhang Yiyi, and Chen Jingdong, who assisted with the fieldwork and sample collection on the Jiangsu coastal mudflat. Special thanks are extended to Dr. Y. Yang for help with the grain-size measurements in the laboratory, and Professor Zhu Jianrong for suggestions and comments on an early version of the original text. The authors thank two anonymous reviewers for constructive suggestions and comments.

References

Andersen, T. J., Fredsoe, J., Pejrup, M. 2007. In situ estimation of erosion and deposition thresholds by Acoustic Doppler Velocimeter (ADV). Estuarine, Coastal and Shelf Science 75(3), 327–336.

Andersen, T. J., Pejrup, M., Nielsen, A. A. 2006. Long-term and high-resolution measurements of bed level changes in a temperate, microtidal coastal lagoon. Marine Geology 226(1), 115–125.

Bass, S.J., Aldridge, J.N., McCave, I.N., Vincent, C.E. 2002. Phase relationships between fine sediment suspensions and tidal currents in coastal seas. Journal of Geophysical Research 107 (C10), 3146.

Cancino, L., Ramiro, N., 1999. Hydrodynamic and sediment suspension modeling in estuarine systems part I: description of the numerical models. Journal of Marine Systems 22, 105–116.

Cheng, P., Wilson, R.E., 2008. Modeling sediment suspensions in an idealized tidal embayment: importance of tidal asymmetry and settling lag. Estuaries and Coasts 31, 828–842.

Christie, M.C., Dyer, K.R., Turner, P., 1999. Sediment Flux and Bed Level measurements from a Macro Tidal Mudflat. Estuarine, Coastal and Shelf Science

49(5), 667–688.

Christie, M. C., Dyer, K. R., & Turner, P. 2000. Observations of long and short term variations in the bed elevation of a macro-tidal mudflat. Proceedings in Marine Science 3, 323-342.

Cancino, L., Neves, R. 1999. Hydrodynamic and sediment suspension modelling in estuarine systems Part I: Description of the numerical models. Journal of Marine Systems 22, 105–116.

Dai, Z. J., Liu, J. T., Lei, Y. P., Zhang, X. L. 2010. Patterns of sediment transport pathways on a headland bay beach-Nanwan beach, South China: a case study. Journal of Coastal Research 26(6), 1096–1103.

Dai, Z. J., Chu, A., Li, W. H., Li, J. F., Wu, H. L. 2013a. Has Suspended Sediment Concentration Near the Mouth Bar of the Yangtze (Changjiang) Estuary Been Declining in Recent Years?. Journal of Coastal Research 29(4), 809–818.

Dai, Z., Liu, J. T., Fu, G., Xie, H. 2013b. A thirteen-year record of bathymetric changes in the North Passage, Changjiang (Yangtze) estuary. Geomorphology 187, 101–107.

Dyer, K.R., 1989. Sediment processes in estuaries: future research requirements. 94(C10), 14327–14339.

Dyer, K.R., 1997. Estuaries—Physical Introduction, second ed. John Wiley and Sons, Chichester 195 pp.

Ellis, K.M., Bowers, D.G., Jones, S.E., 2004. A study of the temporal variability in particle size in a high-energy regime. Estuarine, Coastal and Shelf Science 61,

311–315.
Emery, W.J., Thomson, R.E., 2001. Data Analysis Methods in Physical Oceanography, second ed. Elsevier, Amsterdam 0-444-50757-4, 638 pp.
Jago, C.F., Jones, S.E., 1998. Observation and modelling of the dynamics of benthic fluff resuspended from a sandy bed in the southern North Sea. Continental Shelf Research 18, 1255–1282.
Jago, C.F., Jones, S.E., Sykes, P., Rippeth, T., 2006. Temporal variation of suspended particulate matter and turbulence in a high energy, tide-stirred, coastal sea: relative contributions of resuspension and disaggregation. Continental Shelf Research 26, 2019–2028.
Janssen-Stelder, B. 2000. The effect of different hydrodynamic conditions on the morphodynamics of a tidal mudflat in the Dutch Wadden Sea. Continental shelf research 20(12), 1461–1478.
Johnsen, J., Driscoll, A.M., Johansen, A.O., Lintrup, M.J., 1994. Setup, calibration and verification of a numerical model complex for the study of the spreading of dredging spoils. Report no. 7186. DHI/LIC Joint Venture
Krivtsov, V., Gascoigne, J., Jones, S.E., 2008. Harmonic analysis of suspended particulate matter in the Menai Strait (UK). Ecological Modelling 21, 53–67.
Krögel, F., Flemming, B.W., 1998. Evidence for temperature-adjusted sediment distributions in the backbarrier tidal flats of the east Frisian Wadden sea (southern North sea). In: Alexander, C.R., Davis, R.A., Henry, V.J. (Eds.), tidalites: processes and products: SEPM Spec. Publ., 61, pp. 31–41.

Li. P., Yang, S.L., Milliman, J.D., Xu, K.H., Qin,W.H., Wu, C.S., Chen, Y.P., Shi, B.W., 2012. Spatial, Temporal, and Human-Induced Variations in Suspended Sediment Concentration in the Surface Waters of the Yangtze Estuary and Adjacent Coastal Areas. Estuaries and Coasts 35, 1316–1327.

Liu, J.T., Lin, H.L., 2004. Sediment dynamics in a submarine canyon: a case of river-sea interaction. Marine Geology 207, 55–81.

Liu, J.T., Hung, J.-J., Huang, Y.W., 2009. Partition of suspended and riverbed sediments related to the salt-wedge in the lower reaches of a small mountainous river. Marine Geology 264, 152-164.

Liu, Y.X., Li, M.C., Mao, L., Cheng, L., Chen K.F. 2013. Seasonal pattern of Tidal-Flat Topography along the Jiangsu Middle Coast, China, Using HJ-1 Optical Images. Wetlands. 33(5), 871–886.

Lumborg, U. 2005. Modelling the deposition, erosion, and flux of cohesive sediment through Øresund. Journal of Marine Systems 56, 179–193.

Partheniades, E. 1962. A study of erosion and deposition of cohesive soils in salt water, PhD-thesis, University of California, Berkeley, California, USA.

Partheniades, E. 1965. Erosion and deposition of cohesive soils. Journal of the Hydraulics Division Proceedings of the ASCE 91(HY1), pp. 105–139.

Partheniades, E. 1986. A fundamental framework for cohesive sediment dynamics. In: Mehta, A.J. (Ed.), Estuarine Cohesive Sediment Dynamics. Springer, Berlin, pp. 219–250.

Partheniades, E. 1993. Turbulence, flocculation and cohesive sediment dynamics. In:

A.J. Mehta (Ed.), Nearshore and Estuarine Cohesive Sediment Transport. Am.Geophys. Uion, Washington, DC, pp. 40–59.

Pratolongo, P.D.; Perillo, G.M., and Piccolo, M., 2010. Combined effects of waves and plants on a mud deposition event at a mudflatsaltmarsh edge in the Bah´ıa Blanca estuary. Estuarine, Coastal and Shelf Science, 87(2), 207–212.

Ren, M.E., Zhang, R.S., Yang, J.H., 1985. Effect of typhoon no. 8114 on coastal morphology and sedimentation of Jiangsu Province PRC. Journal of Coastal Research 1 (1), 21–28.

Ren, M.E., 1986. Tidal mud flat. In: Ren, M.E. (Ed.), Modern Sedimentation in the Coastal and Nearshore Zones of China. China Ocean Press, Beijing, pp. 78–127.

Salehi, M., Strom, K., 2012. Measurement of critical shear stress of mud mixtures in the San Jacinto estuary under different wave and current combinations. Continental Shelf Research, 47, 78–92.

Schoellhamer, D.H., T.E. Mumley, and J.E. Leatherbarrow. 2007. Suspended sediment and sediment-associated contaminants in San Francisco Bay. Environmental Research 105, 119–131.

Shi, B.W., Yang, S.L., Wang, Y.P., Bouma, T.J., Zhu, Q., 2012. Relating accretion and erosion at an exposed tidal wetland to the bottom shear stress of combined current–wave action. Geomorphology 138, 380–389.

Shi, B.W., Yang, S.L., Wang, Y.P., Yu, Q., Li, M.L. 2014. Intratidal erosion and deposition rates inferred from field observations of hydrodynamic and sedimentary processes: A case study of a mudflat–saltmarsh transition at the

Yangtze delta front. Continental Shelf Research 90, 109–116

Stanev, E.V., Brink-Spalink, G., Wolff, J.-O., 2007. Sediment dynamics in tidally dominated environments controlled by transport and turbulence: a case study for the East Frisian Wadden Sea. Journal of Geophysical Research 112, C04018. doi:10.1029/2005JC003045.

Tian, T., Merico, A., Su, J., Staneva, J., Wiltshire, K., Wirtz, K., 2009. Importance of resuspended sediment dynamics for the phytoplankton spring bloom in a coastal marine ecosystem. Journal of Sea Research 62, 214–228.

van de Kreeke, J., Hibma, A., 2005. Observations on silt and sand transport in the throat section of the Frisian Inlet. Coastal Engineering 52, 159–175.

Velegrakis, A. F., Gao, S., Lafite, R., Dupont, J. P., Huault, M. F., Nash, L. A., Collins, M. B. 1997. Resuspension and advection processes affecting suspended particulate matter concentrations in the central English Channel. Journal of Sea Research 38(1), 17–34.

Wang, X., Ke, X., 1997. Grain-size characteristics of the extant tidal flat sediments along the Jiangsu coast, China. Sedimentary Geology, 112(1), 105–122.

Wang, Y. P., Gao, S., Jia, J.J. 2006. High-resolution data collection for analysis of sediment dynamic processes associated with combined current-wave action over intertidal flats. Chinese Science Bulletin 51 (7): 866–877.

Wang, A.J., Ye, X., Du, X.Q., Zheng, B.X., 2014. Observations of cohesive sediment behaviors in the muddy area of the northern Taiwan Strait, China. Continental Shelf Research(Accepted)

Wang, Y. P., S. Gao, et al. 2012. Sediment transport over an accretional intertidal flat with influences of reclamation, Jiangsu coast, China. Marine Geology 291–294: 147–161.

Weeks, A.R., Simpson, J.H., Bowers, D., 1993. The relationship between concentrations of suspended particulate material and tidal processes in the Irish Sea. Continental Shelf Research 13,1325–1334.

Whitehouse, R.J.S, Soulsby，R.L., Roberts，W. and Mitchener, H.J., 2000. Dynamics of Estuarine Muds: A manual for practical applications. London: Thomas Telford Publications. ISBN 0-7277-2864-4.

Xing, F., Wang, Y., Gao, J., Zou, X., 2010. Seasonal distributions of the concentrations of suspended sediment along Jiangsu coastal sea. Oceanologia et Limnologia Sinica 41(3), 1-10 (in Chinese with English abstract)

Xing, F., Wang, Y. P., Wang, H. V. 2012. Tidal hydrodynamics and fine-grained sediment transport on the radial sand ridge system in the southern Yellow Sea. Marine Geology 291, 192–210.

Yang, S.L., Li, P., Gao, A., Zhang, J., Zhang, W.X., Li, M., 2007. Cyclical variability of suspended sediment concentration over a low-energy tidal flat in Jiao zhou Bay, China: effect of shoaling on wave impact. Geo-Mar. Lett 27, 345–353.

Yang, S.L., Shi, B.W., Ysebaert, T., Luo,X.X., 2012. Wave attenuation at a saltmarsh margin: a case study of an exposed coast on the Yangtze Estuary. Estuaries Coasts 35,169–182.

Yu, Q., Wang, Y.P., Flemming, B., Gao, S., 2012. Tide-induced suspended sediment transport: Depth-averaged concentrations and horizontal residual fluxes. Continental Shelf Research 34, 53–63.

Zhang R.S., 1992. Suspended sediment transport processes on tidal mud flat in Jiangsu Province, China. Estuarine, Coastal and Shelf Science, 35(3), 225–233.

Zheng, L.Y., C.S. Chen, Zhang, F.Y. 2004. Development of water quality model in the Satilla River Estuary, Georgia. Ecological Modelling 178: 457–482.

Zhu, D.K., Ke, X., Gao, S., 1986. Tidal fiat sedimentation of Jiangsu coast. J. Oceanogr. Huanghai Bohai Seas, 4(3): 19–27 (in Chinese with English abstract).

Zhu, Q., Yang, S., Ma, Y. 2014. Intra-tidal sedimentary processes associated with combined wave–current action on an exposed, erosional mudflat, southeastern Yangtze River Delta, China. Marine Geology, 347, 95–106.

Figure captions

Fig. 1. (A) Study area (red box), and (B) magnified area showing the location of the gauging station (black triangle).

Fig. 2. Size distribution of the uppermost 1–2 cm of surface sediment on the Wanggang mudflat, Jiangsu Coast, China, in the period 27–30 April, 2013. Median = median grain size.

Fig. 3. Conceptual diagram of relationship between suspended sediment flux(F) and erosion/deposition(E/D) flux. F: Suspended sediment flux (including erosion flux E and deposition flux D); F_0： Advective flux.

Fig. 4. Time series of water depth (A), current velocity (B), and wind speed (C) during the field study (27–30 April 2013). The dataset for current velocity was derived from ADP-XR, and was depth-averaged. Wind speed and direction were recorded every minute at a marine gauging station near the present observation site.

Fig. 5. Time series of (A) water depth (h, m) and wave height (H, m); (B) salinity (S, PSU) and temperature (T, °C); (C) SSC (suspended sediment concentration, kg/m^3) at heights of 10, 20, and 40 cm above the bed (z denotes the height above the bed); (D) bed-level changes (mm); (E) dry sediment mass; and (F) percentage contribution (%). In Fig.4 (C), the SSC data at heights of 20 and 40 cm above the bed are missing during Tide 1 because of instrument failure.

Fig. 6. Time series of (A) Water depth (m); (B) Bed shear stress due to waves (τ_w, N/m^2); (C) Bed shear stress due to current (τ_c, N/m^2); (D) Bed shear stress under combined current-wave action (τ_{cw}, N/m^2); (E) Erosion flux ($kg/m^2/s$) inferred from in situ measurement of intratidal bed-level changes and predicted by engineering formula, respectively, and (F) Deposition flux ($kg/m^2/s$) inferred from in situ measurement of intratidal bed-level changes and predicted by engineering formula, respectively. In Fig.5 (E) and (F), erosion and deposition flux is average value within 10 minutes.

Fig. 7. Results of the EOF analysis to determine the factors that influence SSC

variability. The eigenvectors and eigenweights of the first three eigenmodes during Tide 1 (A1 and A2), Tide 2 (B1 and B2), Tide 3 (C1 and C2), Tide 4 (D1 and D2), Tide 5 (E1 and E2), and Tide 6 (F1 and F2) are shown. These eigenmodes represent the main information of the original data (cumulative contribution > 85%).

Table captions

Table 1 Summary statistics for water depth (m), salinity (PSU), temperature (°C), dynamic conditions, depth-averaged SSC (kg/m^3), and intratidal bed-level changes (mm). The dynamic conditions include wind speed (m/s), current velocity (U_b, m/s), and wave height (H_s, m).

Table 2 Statistics for erosion flux (E, $kg/m^2/s$), deposition flux (D, $kg/m^2/s$) and advection flux(F, $kg/m^2/s$), and the percentage contributions from erosion (φ_E), deposition (φ_D), and advection (φ_A) flux to suspended sediment concentrations (SSC) in the water column.

Table 1 Summary statistics for water depth (m), salinity (PSU), temperature (°C), dynamic conditions, depth-averaged SSC (kg/m^3), and intratidal bed-level changes (mm). The dynamic conditions include wind speed (m/s), current velocity (U_b, m/s), and wave height (H_s, m).

Tides	Water depth (m)		Salinity (PSU)		Temperature (°C)`		Dynamic conditions						Depth-averaged SSC (kg/m^3)		Intratidal bed-level changes (mm/s)*			
							wind speed (m/s)		U_b (m/s)		H_s (m)				Net erosion		Net accretion	
	Max	Mean	Max	Mean	Max	Mean	Max	Mean	Max	Mean	Max	Mean	Max	Mean	Max	Mean	Max	Mean
Tide 1	1.16	0.92	25.03	23.93	17.32	15.60	8.50	6.08	0.41	0.23	0.11	0.07	1.43	0.66	–0.08	–0.02	0.08	0.02
Tide 2	1.04	0.84	25.37	24.93	15.31	14.27	10.00	8.13	0.52	0.29	0.10	0.07	1.84	1.43	–0.08	–0.03	0.05	0.03
Tide 3	1.28	0.96	25.35	24.78	17.12	15.75	10.10	7.23	0.65	0.22	0.25	0.13	2.84	1.40	–0.05	–0.02	0.03	0.02
Tide 4	0.98	0.76	25.47	25.20	16.05	15.03	7.10	6.05	0.56	0.25	0.08	0.06	1.99	1.30	–0.03	–0.02	0.03	0.02
Tide 5	1.50	1.10	25.37	24.42	16.24	15.65	13.90	9.23	0.35	0.21	0.38	0.20	7.87	4.23	–0.26	–0.05	0.13	0.04
Tide 6	0.77	0.64	24.79	23.96	16.01	15.41	6.10	3.95	0.33	0.21	0.08	0.06	2.32	1.50	0.13	–0.04	0.11	0.04

*The minus sign ("–") denotes erosion.

Table 2 Statistics for erosion flux (E, kg/m^2/s), deposition flux (D, kg/m^2/s) and advective flux(F_0, kg/m^2/s), and the percentage contributions from erosion (φ_E), deposition (φ_D), and advection (φ_A) flux to suspended sediment concentrations (SSC) in the water column.

Tides	Sediment flux (kg/m^2/s)									Percentage contribution (%)*								
	E			*D*			F_0			φ_E			φ_D			φ_A		
	Max	Min	Mean	Max	Min	Mean	Max	Min	Mean	Max	Min	Mean	Max	Min	Mean	Max	Min	Mean
Tide 1	0.04	0	0.01	0.04	0	0.01	0.24	0.05	0.13	+22.06	+1.17	+16.27	–30.42	–1.19	–16.55	+130.42	+77.94	+100.87
Tide 2	0.04	0	0.01	0.03	0	0.01	0.45	0.10	0.26	+20.09	+0.63	+6.10	–16.45	–0.60	–5.20	+116.45	+79.91	+99.97
Tide 3	0.03	0	0.01	0.02	0	0.01	0.60	0.13	0.32	+12.12	+0.64	+4.63	–8.24	–0.24	–4.63	+108.24	+87.88	+100.08
Tide 4	0.01	0	0.01	0.02	0	0.01	0.33	0.09	0.20	+9.07	+1.01	+5.50	–11.12	–0.95	–5.87	+111.12	+90.93	+100.02
Tide 5	0.14	0	0.02	0.14	0	0.02	3.21	0.02	1.02	+113.61	+0.08	+5.17	–24.51	–0.16	–4.66	+245.25	+58.68	+100.51
Tide 6	0.07	0	0.02	0.06	0	0.02	0.32	0.03	0.19	+62.05	+1.01	+13.41	–34.27	–1.38	–11.70	+134.27	+37.95	+99.95

*A minus sign ("–") denotes a negative contribution to the suspended sediment concentration in the water column; a plus sign ("+") denotes a positive contribution to the suspended sediment concentration in the water column.

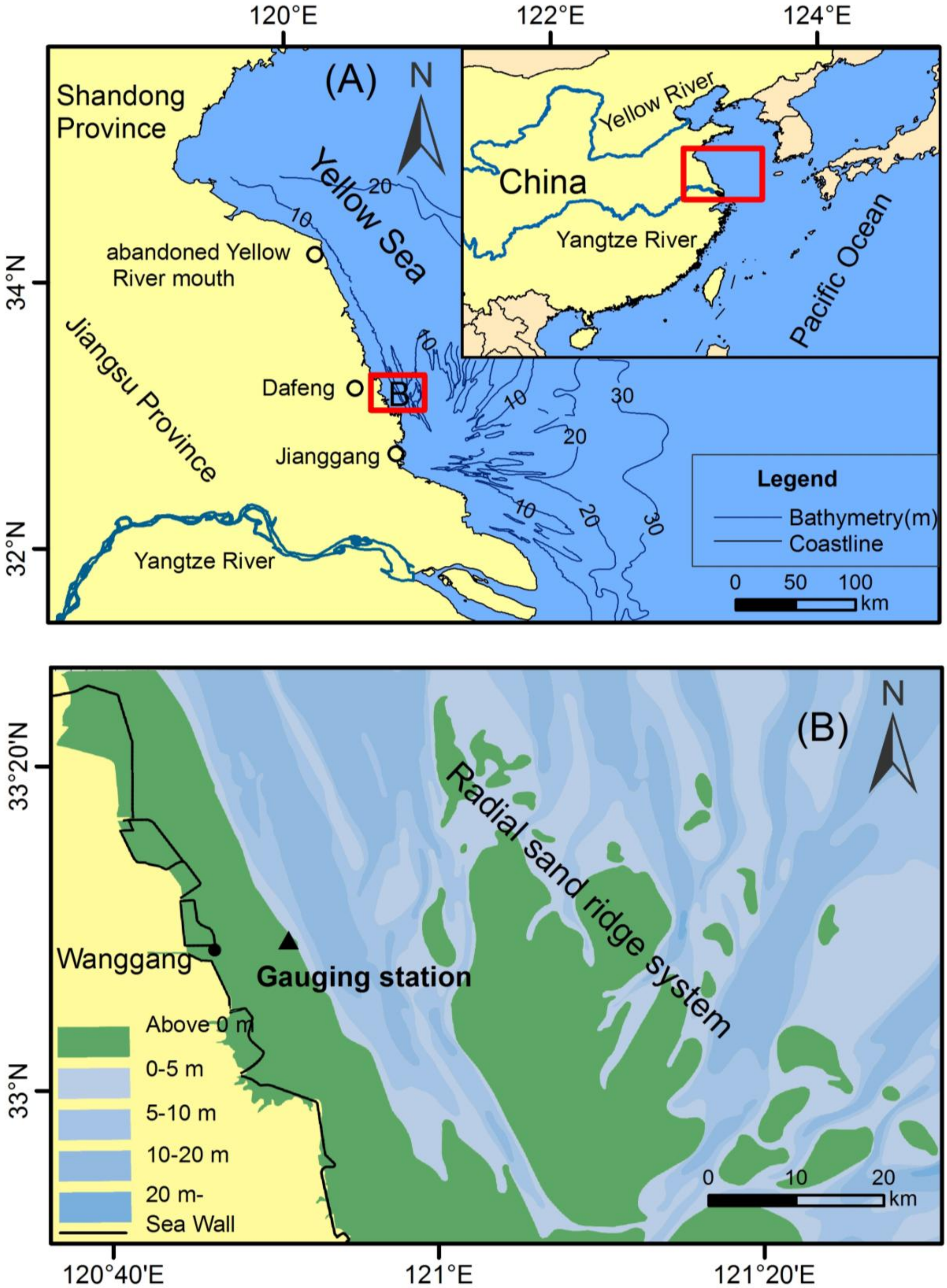

Fig. 1. (A) Study area (red box), and (B) magnified area showing the location of the gauging station (black triangle).

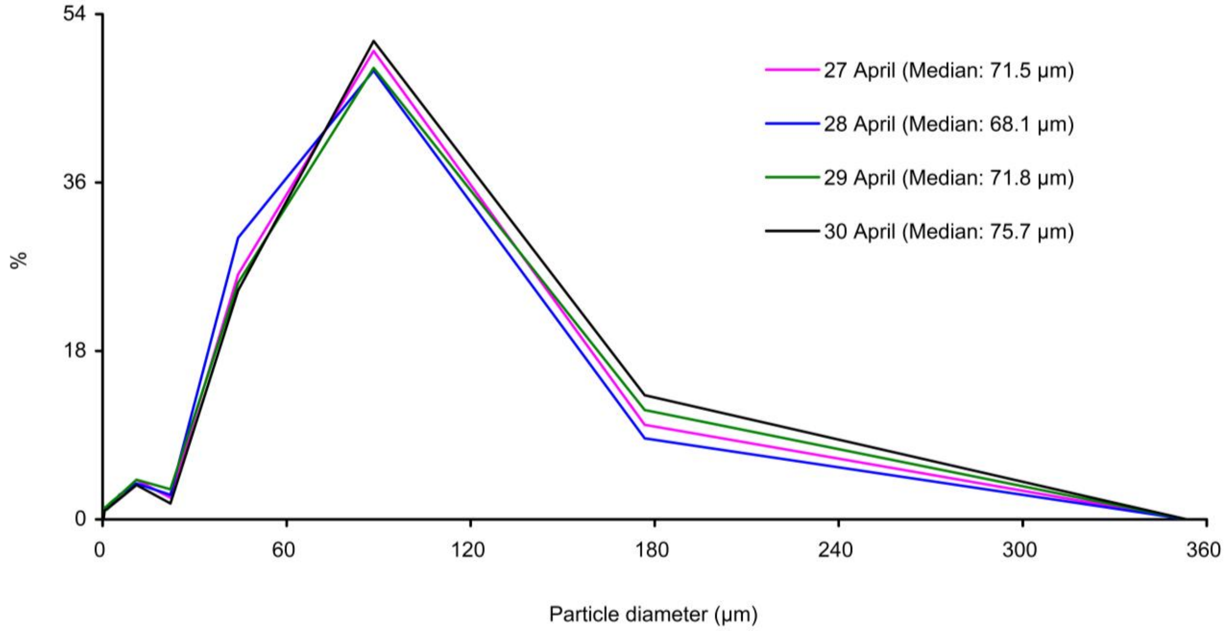

Fig.2. Size distribution of the uppermost 1–2 cm of surface sediment on the Wanggang mudflat, Jiangsu Coast, China, in the period 27–30 April, 2013. Median = median grain size.

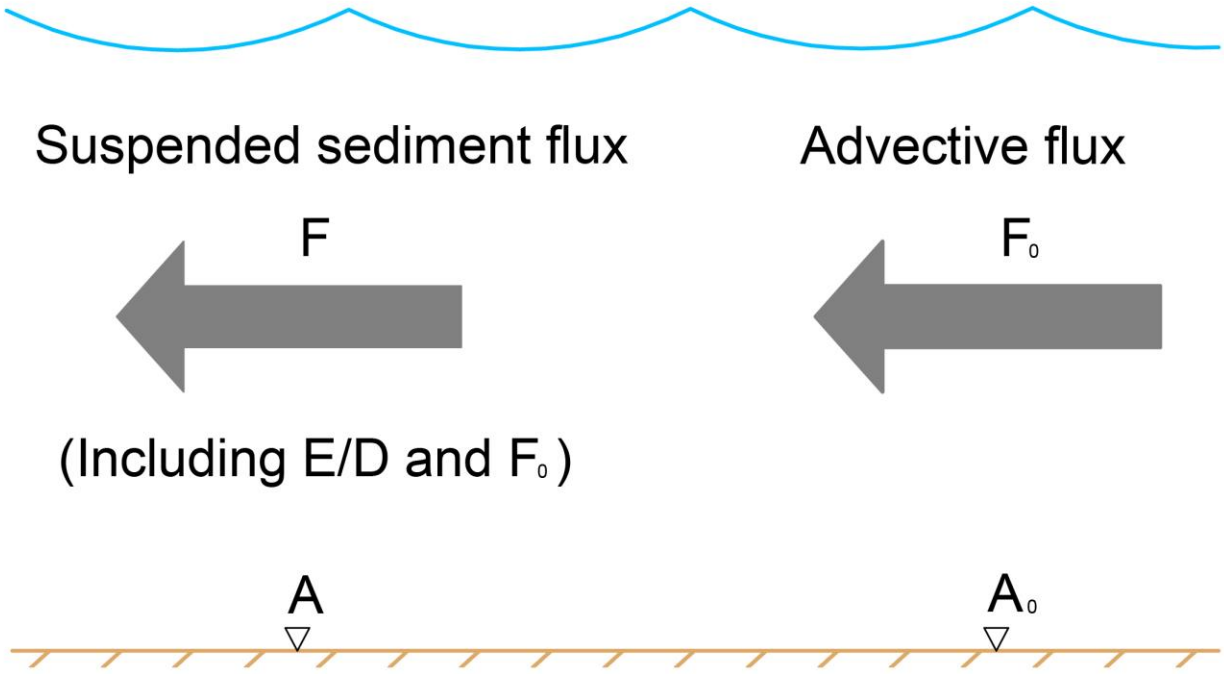

Fig.3. Conceptual diagram of relationship between suspended sediment flux(F), erosion/deposition(E/D) flux and advective flux (F_0). F: Suspended sediment flux (including erosion flux E and deposition flux D); F_0：Advective flux.

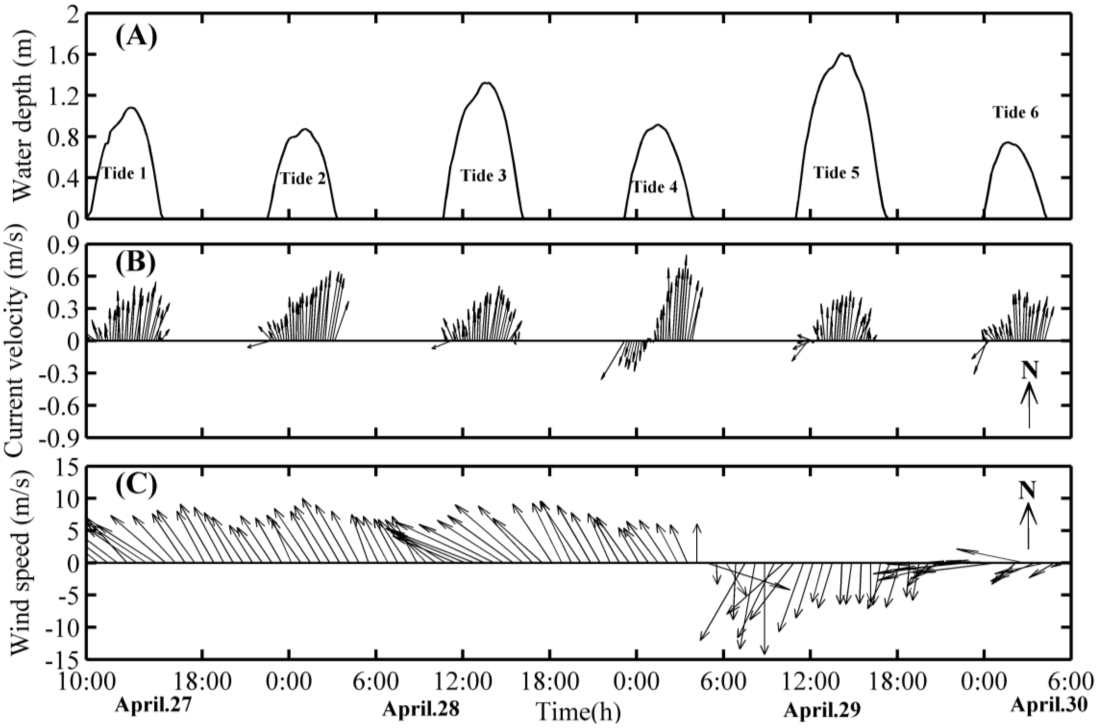

Fig.4. Time series of water depth (A), current velocity (B), and wind speed (C) during the field study (27–30 April 2013). The dataset for current velocity was derived from ADP-XR, and was depth-averaged. Wind speed and direction were recorded every minute at a marine gauging station near the present observation site.

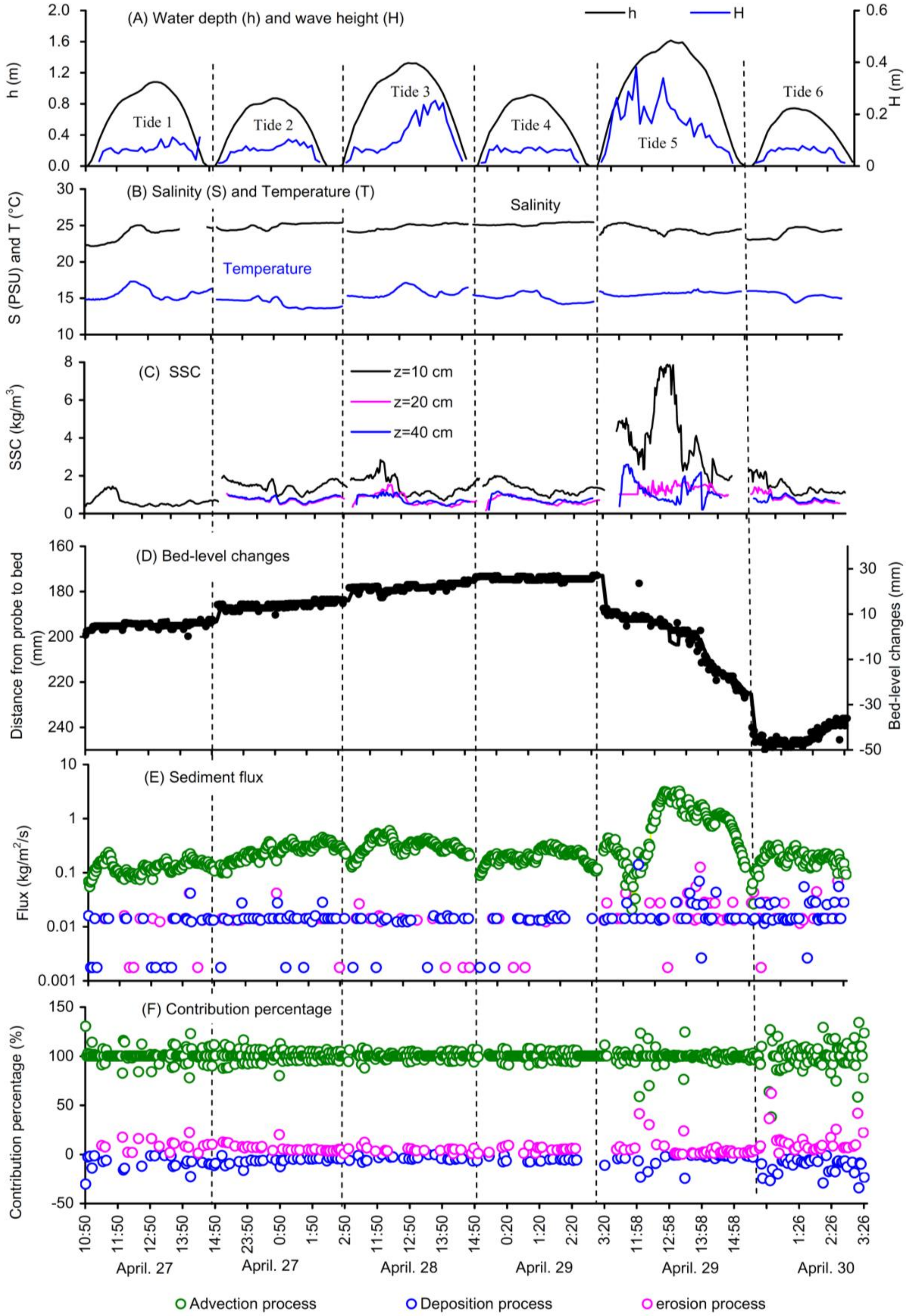

Fig. 5. Time series of (A) water depth (h) and wave height (H); (B) salinity (S, PSU) and temperature (T, °C); (C) SSC (suspended sediment concentration, kg/m^3) at heights of 10, 20, and 40 cm above the bed (z denotes the height above the bed); (D) bed-level changes (mm); (E) Sediment flux; and (F) percentage contribution (%). In Fig.4 (C), the SSC data at heights of 20 and 40 cm above the bed are missing during Tide 1 because of instrument failure.

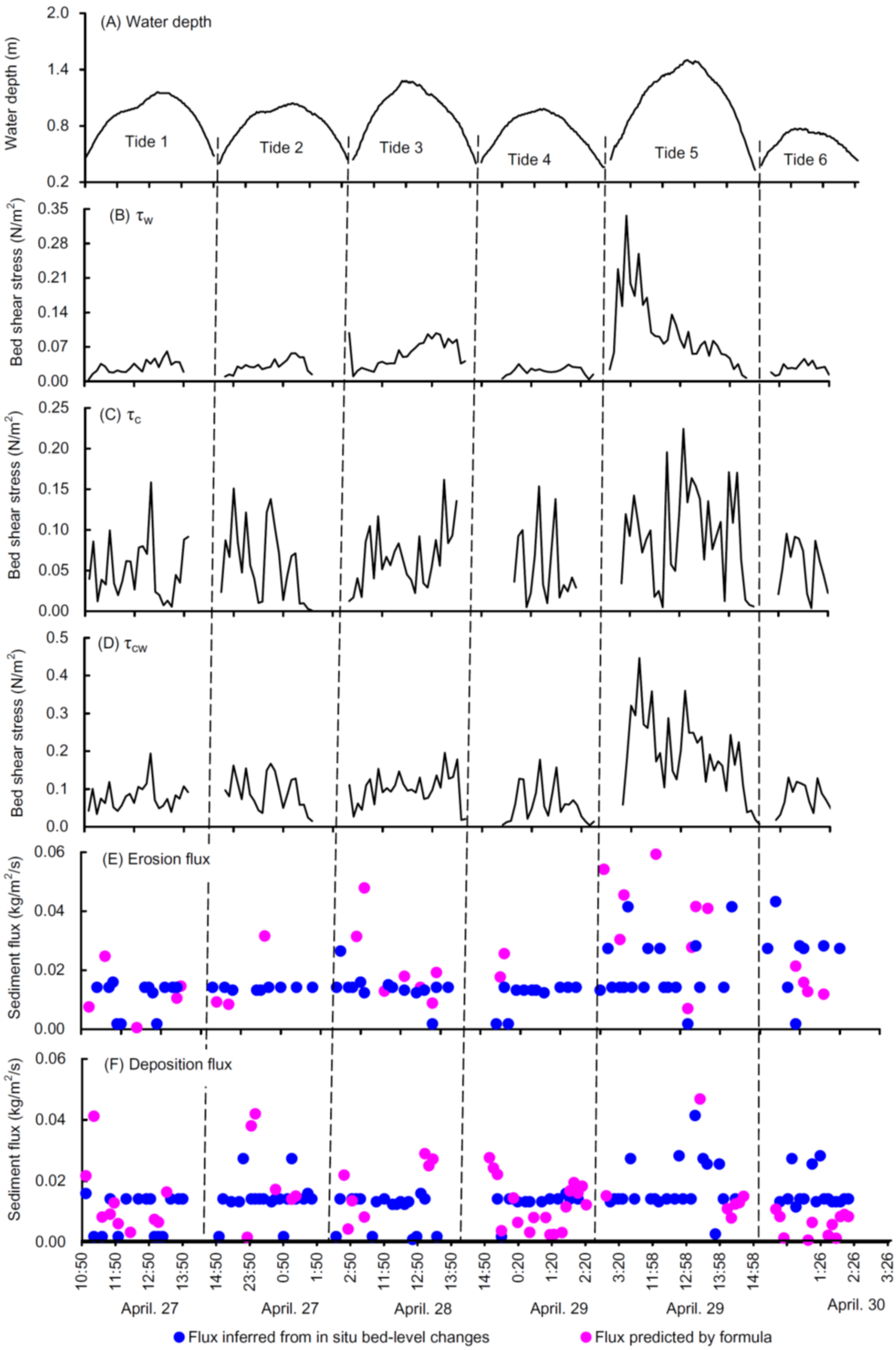

Fig.6. Time series of (A) Water depth (m); (B) Bed shear stress due to waves (τ_w, N/m^2); (C) Bed shear stress due to current (τ_c, N/m^2); (D) Bed shear stress under combined current-wave action (τ_{cw}, N/m^2); (E) Erosion flux (kg/m^2/s) inferred from in situ measurement of intratidal bed-level changes and predicted by engineering formula, respectively, and (F) Deposition flux (kg/m^2/s) inferred from in situ measurement of intratidal bed-level changes and predicted by engineering formula, respectively. In Fig.5 (E) and (F), erosion flux and deposition flux are average value within 10 minutes.

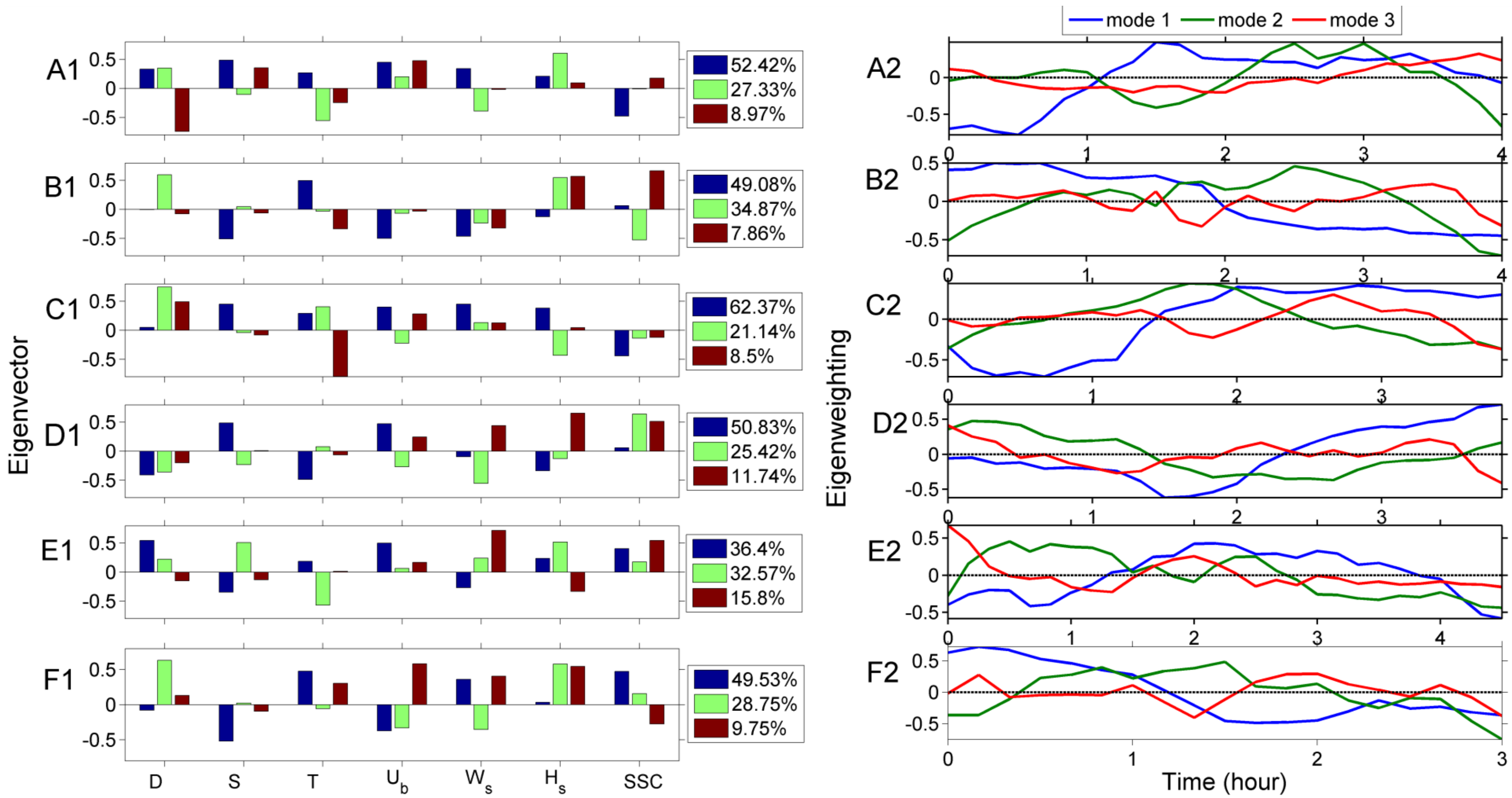

Fig.7. Results of the EOF analysis to determine the factors that influence local SSC variability. The eigenvectors and eigenweights of the first three eigenmodes during Tide 1 (A1 and A2), Tide 2 (B1 and B2), Tide 3 (C1 and C2), Tide 4 (D1 and D2), Tide 5 (E1 and E2), and Tide 6 (F1 and F2) are shown. These eigenmodes represent the main information of the original data (cumulative contribution > 85%).